ECS Journal of Solid State
Science and Technology

The Electrochemical Society
Advancing solid state & electrochemical science & technology

Electronic Structure, Optical and Thermal Response of Lead-Free $RbAuBr_3$ and $RbAuBr_4$ Perovskites for Renewable Energy Applications

ECS Journal of Solid State Science and Technology, 2022 **11** 123003
2162-8777/2022/11(12)/123003/7/$40.00 © 2022 The Electrochemical Society ("ECS"). Published on behalf of ECS by IOP Publishing Limited

Electronic Structure, Optical and Thermal Response of Lead-Free $RbAuBr_3$ and $RbAuBr_4$ Perovskites for Renewable Energy Applications

Junaid Munir,[1] Muhammad Mustafa,[1] Hamza Naeem,[2] Masood Yousaf,[2] E. F. El-Shamy,[3] and Quratul Ain[4,z]

[1]*Department of Physics, Riphah International University, Lahore, Pakistan*
[2]*Department of Physics, University of Education, Lahore, Pakistan*
[3]*Research Center for Advanced Materials Science (RCAMS), King Khalid University, P.O. Box 9004, Saudi Arabia*
[4]*Department of Physics, University of Management and Technology, Lahore, Pakistan*

The presence of toxic lead in the perovskites is the major hurdle in commercializing these novel materials-based devices. The first principles calculations have been conducted to investigate the electronic structure, optoelectronic, and transport properties of lead-free $RbAuBr_3$ and $RbAuBr_4$ perovskites. Modified Becke-Johnson approximation is used to evaluate the accurate band structures for both compounds. The calculated energy-volume curves and the negative formation energy values confirm their stability. The band structure profile shows a semiconductor nature of both compounds with bandgap values of 0.77 eV and 2.32 eV for $RbAuBr_3$ and $RbAuBr_4$, respectively. The density of states graphs endorsed the band structure results. The optical response is calculated in terms of real and imaginary parts of the dielectric function, refractive index, and energy loss parameters. The maximum absorption is achieved in the infrared region for $RbAuBr_3$ and the visible region for $RbAuBr_4$. The thermoelectric response is also computed and a high ZT value of 0.96 is achieved for $RbAuBr_3$, while a moderate value of 0.60 is obtained for $RbAuBr_4$ at 800 K. The calculated properties reveal the potential of studied lead-free perovskites for thermoelectric and optoelectronic applications.
 [DOI: 10.1149/2162-8777/aca795]

Manuscript submitted September 27, 2022; revised manuscript received November 22, 2022. Published December 8, 2022.

The shortage and high demand for consumable energy in the advanced global world motivate researchers to discover new renewable energy sources.[1] Waste heat and Sunlight are significant renewable energy sources, which can be directly converted into light energy by thermoelectric generators and solar cells. The choice of materials has a fundamental role in determining the efficiency of thermoelectric and optoelectronic devices.[2–7] A huge part of the Earth's crust contains Perovskites, a class of materials that contains an extensive range of substances from insulators to superconductors. The perovskite materials, which have the general formula ABX_3, are excellent candidates for the creation of various optoelectronic devices because they offer exceptional optoelectronic capabilities.[8–10] The band gap of most ABX3-type perovskites falls in the visible region, which attracts researchers to explore their features with a wide range of applications in solar cells.[11,12] The exceptional optoelectronic characteristics of hybrid lead-based perovskites provide a wide range of applications in the field of photonics, such as lasers and light-emitting diodes.[12–14] Perovskite materials are particularly famous in the photovoltaic field due to their high power conversion efficiency, which has increased from 3.8%[15] to 22.7%[16] in recent years. Despite their attractive features, perovskites are facing major challenges in their commercialization because of the toxic nature of lead and the instability of their structures against the temperature and air/moisture.[17–20] The instability problem can be addressed by carbon encapsulation, multication substitution, and incorporation of hydrophobic moieties.[21] The toxicity of perovskites can be encountered by replacing Pb with non-toxic elements.[22] The replacement of Pb is done with the group-IVA no-toxic elements such as Ge and Sn. However, it is noted that the replacement of Pb with Sn results in less stable perovskites.[23] The substitution of Ge in place of Pb causes the reduction of optical conductivity, light absorption, and dielectric constant, which decreases photovoltaic performance.[20] Inorganic halide-perovskites are presently considered to be a mainstream research topic due to the absence of sensitive organic components.[24–26] Although inorganic halide perovskites show good optoelectronic properties, they have many limitations.[27,28] Recently, $CsPbX_3$ (X=I, Cl, Br) perovskites revealed high thermal stability than the other perovskite materials.[29,30] In addition, a large amount of experimental and theoretical work has been done widely in the recent past to explore perovskite properties.[31–35] Although there are many perovskites with diverse properties have been reported in the literature, a desire to discover more useful perovskite materials for thermoelectric devices is still growing in the research community. In the current report, a comprehensive investigation of the important properties of $RbAuBr_3$ and $RbAuBr_4$ is done. To the best of our knowledge up till now, there is no simulation work has been carried out on $RbAuBr_3$ and $RbAuBr_4$ perovskites to discover their potential in thermoelectric and optoelectronic applications. The present work comprises the mechanical and structural stability along with the calculation of ground-state electronic structure, optoelectronic and thermoelectric properties of studied perovskite materials.

Research Methodology

To determine the physical properties of perovskites, we used density functional theory (DFT) based calculations with a full potential linearized plane wave (FP-LAPW) study executed in the WIEN2k code.[36] FP-LAPW is used to find the solution of the Kohn–Sham equation and results in the determination of ground-state properties of non-interrelating systems. To correctly calculate the electronic response of selected compounds, we implemented Trans-Blaha modified Becke-Johnson (mBJ) exchange-correlation potential.[37,38]

$$v_{\sigma,x}^{mBj}(r) = c\,v_{x,\sigma}^{BR}(r) + (3c-2)\frac{1}{\pi}\sqrt{\frac{5}{6}}\sqrt{\frac{t_\sigma(r)}{\rho_\sigma(r)}} \quad [1]$$

Where t_σ is the kinetic energy density, ρ_σ represents the electron density, and $v_{\sigma,x}^{mBj}$ stands for Becke Roussel's potential of bulk crystalline materials.[39]

$$c = \alpha + \beta\left(\frac{1}{V_{cell}}\int_{cell}\frac{\nabla n(\vec{r})'}{n(\vec{r})'}d^3(\vec{r})'\right)^{\frac{1}{2}} \quad [2]$$

where V_{cell} is cell volume. The α and β parameters are chosen in the extensive range of solids to fit the bandgap. The WIEN2k code is used to calculate the optoelectronic properties of the studied

[z]E-mail: ainnie357@yaoo.com

compounds, while thermoelectric properties are computed with the help of the BoltZTrap code.[40] The wave function of the Kohn–Sham equation is expended inside the sphere as atomic-like orbitals and in the interstitial region as a plane wave. During the calculations, basis set extension is managed with $R_{MT}K_{max} = 7$ and spherical harmonics are set to $l_{max} = 10$. Self-consistency for charge and energy is attained up to 0.001 e/a. and 0.0001 R_y per unit cell, respectively. In Brillouin Zone, the integration over the K-space to achieve self-consistency for a Bloch correction is done with 1200 k-points. The ground-state properties were calculated using optimized lattice parameters. Constant relaxation time (τ) approximation is used for the calculation of transport properties implemented through the BoltzTrap code.[41] The thermoelectric parameters are computed with the help of the following relations:

$$S = \frac{8\pi^2 K_B^2}{3e^2h^2}(m_x^* m_y^* m_z^*)^{\frac{1}{3}} N_v^{\frac{2}{3}} T\left(\frac{\pi}{3n}\right)^{\frac{2}{3}} \quad [3]$$

$$m_i^* = \frac{\int e^{\frac{-dE(k)}{K_B T}} m_b^*(k) d(k)}{\int e^{\frac{-dE(k)}{K_B T}} d(k)} \quad [4]$$

$$m_b^* = \frac{\hbar^2}{\frac{\partial^2 E(k)}{\partial K^2}} \quad [5]$$

Where N_v, k, h, K_B, n, T, E(k), m_i, and m_b are the band degeneracy, the electric charge, the Boltzmann constant, the plank constant, the carrier concentration, the temperature, the band energy, the mass components, and band mass, respectively.[42]

Result and Discussion

Crystal structure.—The studied monoclinic Perovskite type compounds $RbAuBr_3$ and $RbAuBr_4$ belong to the space group C2/m and P2_1/c. The unit cell crystal structure of both materials is drawn with XCrySDen and presented in Fig. 1. The bond lengths and ionic radii are the main factors that determine the material structure's stability and effectiveness. Cations and anions arrangement in materials have an essential role in defining the band structure, stability and materials performance, as well as definite applications in the practical world. To ground-state properties of studied compounds are calculated by using the optimized lattice parameters. Optimization of the structure was done with the help of Birch-Murnaghan's equation of state,[43] which is also used to describe the variations in the total energy of the system corresponding to the volume.

$$E(V) = E_o + \frac{9B_{oV_o}}{16}\left\{\left[\left(\frac{V_o}{V}\right)^{2/3} - 1\right]B_{o+}\left[\left(\frac{V_o}{V}\right)^{2/3} - 1\right] \times \left[6 - 4\left(\frac{V_o}{V}\right)^{2/3} - 1\right]\right\} \quad [6]$$

Here V_0 is the unit cell volume, B_0 is an equilibrium bulk modulus, B'_0 is the derivative of the bulk modulus and E_0 is the minimized energy at the ground state. The calculated optimization graph of $RbAuBr_3$ and $RbAuBr_4$ are shown in Fig. 2.

To determine the possibility of synthesizing the materials, we calculated the formation energy for both materials. It is the difference between total energy with the energy of the individual atoms. The negative value of formation energy corresponds to the stable nature of the material and the positive value of energy indicates the spontaneous nature of the material and hence instability.[44] The calculated ground state parameters are presented in Table I.

Electronic structure.—The range of energy levels possessed by the electrons in a material is illustrated with an electronic band structure. It is the most crucial factor in determining the internal characteristics of any material.[45] The electronic structure is also used to accurately explain the electronic transitions due to the distribution of electrons inside the bands. We have investigated the electronic band structures of $RbAuBr_3$ and $RbAuBr_4$ at equilibrium along the asymmetry lines [Γ-H-N-Γ] in the 1st Brillouin zone, as shown in Fig. 3. The unoccupied Fermi level demonstrates the semiconducting nature of both compounds. Electronic band curves for both compounds reveal that the lowest point of the conduction band and the highest point of the valence band lay at the same symmetry points (H-H) of the Brillouin zone generating a direct band gap of 0.77 eV and 2.32 eV for $RbAuBr_3$ and $RbAuBr_4$, respectively.

To further explanation of the band gap profile for studied compounds is given with the total density of states (DOS). The qualitative description of both conduction and valence bands, along with the associated energy states, is provided with DOS. The total DOS graphs are presented in Fig. 3. Both graphs of DOS express the same result as band structure plots and confirm the semiconductor behavior of both compounds. The highest peaks in the valence band correspond to the maximum contribution of d-orbitals of Au atoms. To study in deep the individual role of elements in total DOS, we have simulated and plotted the partial density of states (PDOS) as shown in Fig. 4.

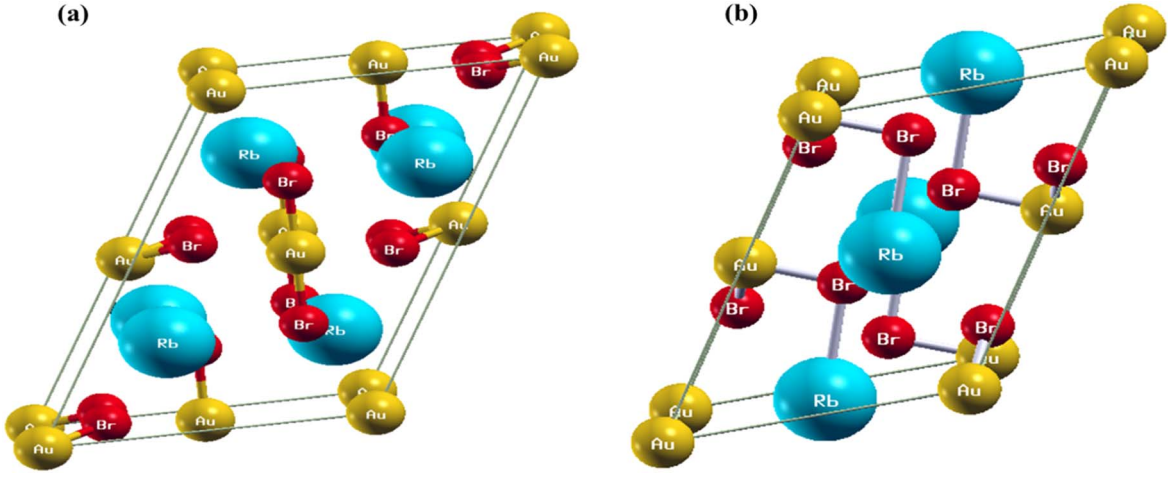

Figure 1. Crystal structure of (a) $RbAuBr_3$ and (b) $RbAuBr_4$ perovskites.

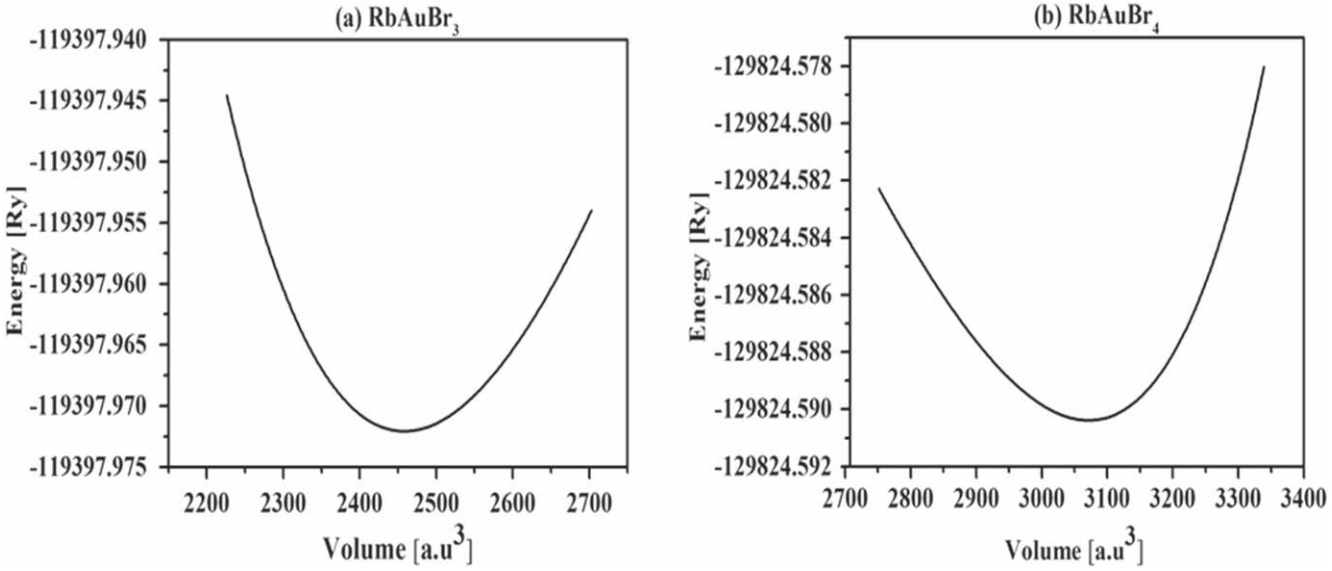

Figure 2. The volume optimization graphs of (a) $RbAuBr_3$ and (b) $RbAuBr_4$ perovskites.

Table I. Optimized lattice parameters of $RbAuBr_3$ and $RbAuBr_4$.

	Lattice parameters					
Compounds	Lattice Constants (Å)	V_o	B(GPa)	**B′**	$E_o(R_y)$	E_f (eV atom^{-1})
$RbAuBr_3$	a = b = 7.26, c = 8.24	2458.2570	27.9318	7.0893	−119397.97207	−1.992
$RbAuBr_4$	a = 6.17, b = 7.45, c = 10.60	2558.2370	29.9318	8.0893	−129824.57807	−1.756

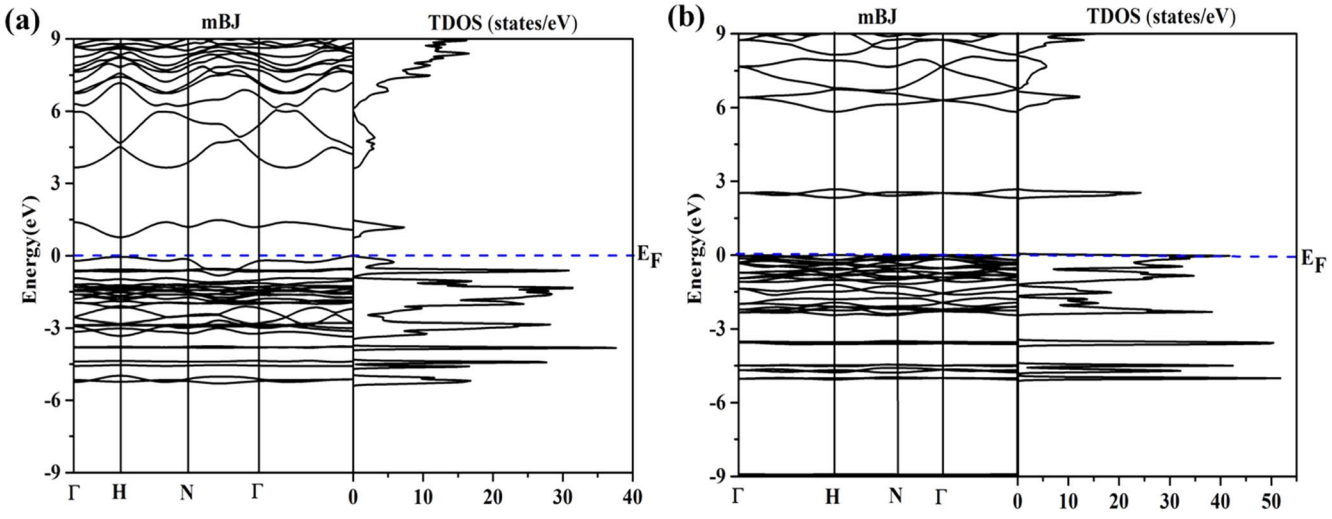

Figure 3. Band structure and total density of states (a) $RbAuBr_3$ and (b) $RbAuBr_4$.

For $RbAuBr_3$, the d-states of Rb, Au, and Br express the maximum influence in the valence band, while the d-states of Au have a major contribution in the conduction band. For $RbAuBr_4$, d-states of Rb and Au show major influence in the valence band and d-states of Rb express the maximum influence in the conduction band. The contribution of p-states of Br is also present in both bands but is comparatively low concerning other elements.

Optical properties.—Materials' optical response is essential for their possible applications in optoelectronic and solar cells. The dielectric function plays a crucial role in determining the accurate optical properties of materials such as absorption, refractive index, and energy loss.[46] The material's ability to harvest light energy can be determined by dielectric function. The calculation of dielectric function i.e. $\varepsilon(\omega) = \varepsilon_1(\omega) + \varepsilon_2(\omega)$ also provides a path to calculate other optical properties.[47] The $\varepsilon_1(\omega)$ and $\varepsilon_2(\omega)$ signify the real and imaginary parts of the dielectric function.

The $\varepsilon(\omega)$ can be calculated with the help of momentum matrix elements by using the following Kramer-kroning relation.[48]

$$\varepsilon_1(\omega) = 1 + \frac{2p}{\pi}\int_0^{\infty} \frac{\omega'\varepsilon_2(\omega')}{\omega'^2 - \omega^2} d\omega \qquad [7]$$

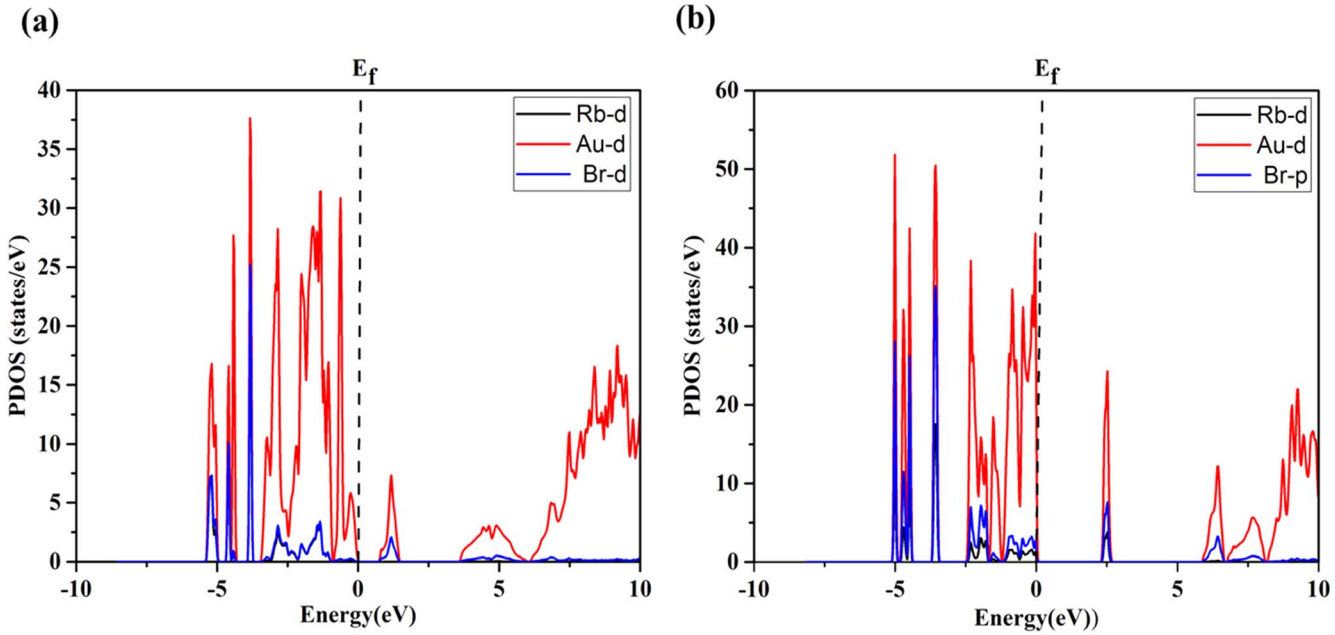

Figure 4. The calculated PDOS of (a) $RbAuBr_3$ and (b) $RbAuBr_4$.

$$\varepsilon_2(\omega) = \frac{8}{2\pi\omega^2} \sum_{nn'} \int |p_{nn'}|^2 \frac{dS_k}{\nabla \omega_{nn'(k)}} \quad [8]$$

Here $p_{nn'}$ (K) is the dipole matrix element, P is the Cauchy principle and $\omega_{nn(k)'}$ is the energy difference. The real part $\varepsilon_1(\omega)$ reports the scattering power and the imaginary part of the epsilon $\varepsilon_2(\omega)$ of the dielectric constant shows the loss of energy and the ability to absorb energy in any material.[49]

The calculated graphs of $\varepsilon_1(\omega)$ for both compounds are shown in Fig. 5a. The $\varepsilon_1(0)$ (static values) are 6.6 for $RbAuBr_3$ and 2.8 for $RbAuBr_4$ with mBJ potential. The first and highest peak is observed at 1.1 eV for $RbAuBr_3$ and 2.55 eV for $RbAuBr_4$. After the peak values, a rapid decrease is observed, leading to the peak of negative values i.e. 1.6 eV for $RbAuBr_3$ and 4.7 eV for $RbAuBr_4$, indicating no propagation of electromagnetic waves. The negative values of the real dielectric $\varepsilon_1(\omega)$ constant demonstrate the metallic behavior of the studied compound.[50] Suddenly after negative peaks, there is a rise in $\varepsilon_1(\omega)$ values, which again become negative after 12 eV.

The peaks in the ε_2 (ω) part of the dielectric function correspond to the electronic transition from occupied to unoccupied energy states, as displayed in Fig. 5b. The incident photons have low energy to transfer electrons from the valence band to the conduction band, so there is no electrons transition from 0 eV to 0.81 eV for $RbAuBr_3$ and 0 eV to 2.5 eV for $RbAuBr_4$ with mBJ potential. The transition of electrons starts from 0.73 eV and 1.76 eV for $RbAuBr_3$ and $RbAuBr_4$, respectively, and this energy is called the threshold energy for transition.[51] It is observed from Fig. 5b that after getting threshold frequency, the value of imaginary epsilon $\varepsilon_2(\omega)$ increases and gains a maximum sharp peak at 1.3 eV for $RbAuBr_3$. For $RbAuBr_4$, the first peak is noted at 2.9 eV and the maximum peak is observed at 4.6 eV. The peaks indicate the maximum absorption of incident light in the visible region, where the light scattering is minimum for both compounds. The variations in $\varepsilon_2(\omega)$ values at the higher energy range have occurred due to different rates of intra-band and inter-band transitions.[52] These peaks originate from the electronic transitions when the electric field is constant.

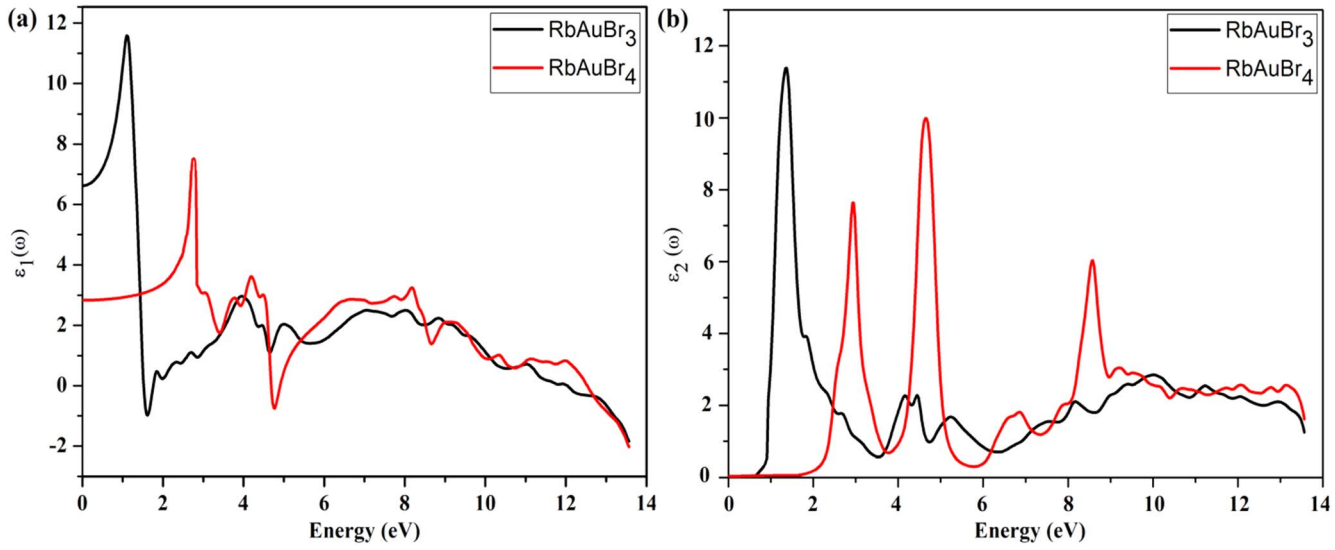

Figure 5. The real (a) and imaginary (b) parts of the dielectric function of $RbAuBr_3$ and $RbAuBr_4$.

Another vital consideration is the refractive index n (ω) in optical properties. The n(ω), in terms of impurity and wavelength, gauges the transparency rate and light dispersion through its substituent elements.[53] According to Fig. 6a, the calculated static values n(0) are 2.6 and 1.6 for $RbAuBr_3$ and $RbAuBr_4$, respectively. The highest peaks of refractive index are found at 1.1 eV and 2.6 eV for $RbAuBr_3$ and $RbAuBr_4$, respectively. Small bandgap and rising photon energy cause the refractive spectra's magnitude to increase. Figure 6b displays reflectivity for $RbAuBr_3$ and $RbAuBr_4$ regarding the photon energy, which ranges from 0 eV to 14 eV. The highest peak is seen at 1.4 eV for $RbAuBr_3$ and 4.7 eV for $RbAuBr_4$ with mBJ potential.

Figure 6b demonstrates energy loss that depends on the photon energy. It expresses the wasted energy during the fast electronic transition. The minimum energy loss means the maximum absorption. The maximum peaks of eloss are observed at 2.87 eV and 4.9 eV for $RbAuBr_3$ and $RbAuBr_4$, respectively. After that, there is a fluctuation in both cases due to inner-band transitions. $RbAuBr_3$ has the least energy losses compared to $RbAuBr_4$, so it seems a possible candidate for photonic absorption.

Thermoelectric properties.—The thermoelectric response in terms of electrical and thermal conductivities, Seebeck coefficient, and figure of merit (ZT) have been calculated using classical Boltzmann transport theory (CBT) as applied in the BoltzTrap code.[54,55] The material's thermal power must increase when thermal conductivity has a minimum value while electrical conductivity and Seebeck coefficient have maximum values. The relation of electrical conductivity to thermal conductivity is explicit by the Wiedemann–Franz Law.[56] Material's effectiveness for thermoelectric (TE) devices can be estimated with the help of a figure of merit.[57]

Figure 7a represents the electrical conductivity of both compounds. The value of electrical conductivity at 50 K is 1.77×10^{19} (S m^{-1}) for $RbAuBr_3$ and 7.6×10^{18}(S m^{-1}) for $RbAuBr_4$. By increasing the temperature from 50 K to 800 K, the electrical conductivity shows small variations for both materials. At 800 K, the electrical conductivity reaches the value of 1.46×1019(S m^{-1}) for $RbAuBr_3$ and 7.6×1018(S m^{-1}) for $RbAuBr_4$. The electrical conductivity of $RbAuBr_3$ is relatively higher than $RbAuBr_4$ at every point because electrons require less energy to reach the conduction band because of the small bandgap. Thermal conductivity is also an essential property in studying the material's response to increasing temperature.[58] The temperature-dependent increasing thermal conductivity values of materials show their semiconductor behavior.[59]

The calculated thermal conductivity of both compounds is presented in Fig. 7b. The computed thermal conductivity at 50 K is 1.85×10^{13} (W.K^{-1} m^{-1}) for $RbAuBr_3$ and 8.2×10^{12} (W.K^{-1} m^{-1}) for $RbAuBr_4$. Thermal conductivity value increases linearly from 50 K to 800 K for both compounds. At 800k, the calculated thermal conductivity values are 3.2×10^{14} (W.K^{-1} m^{-1}) for $RbAuBr_3$ and 1.7×10^{14} (W.K^{-1} m^{-1}) for $RbAuBr_4$. The reason for the small increase in thermal conductivity of $RbAuBr_4$ may be related to its large band gap as compared to $RbAuBr_3$. Seebeck coefficient is the magnitude of induced thermoelectric voltage due to temperature gradient.[60] The Seebeck coefficient values are computed for both compounds and presented in Fig. 8a. The maximum calculated value of the Seebeck coefficient for $RbAuBr_3$ is 1.28×10^{-4} (VK^{-1}) at 600 K, while for $RbAuBr_4$ is 1.34×10^{-4} (VK^{-1}) at 700 K. It is observed that by increasing the temperature from 50 K to 800 K, the Seebeck values also increase for both studied compounds.

The figure of merit (ZT) is the degree that is used to measure the material's efficiency with a temperature gradient.[61] The figure of merit (ZT) values are calculated for both compounds and presented in Fig. 8b. The calculated maximum value of the figure of merit (ZT) for $RbAuBr_3$ is 1. 16 at 50 K, while for $RbAuBr_4$ is 0.24 at 50 K with mBJ potential. The ZT value for $RbAuBr_3$ decreases (100 K–300 K) and then gradually increases (200 K–800 K). At 800 K, the ZT value of 0.96 is obtained for $RbAuBr_3$. In the case of $RbAuBr_4$, the ZT value gradually increases from 100 K to 800 K and the maximum value of 0.60 is achieved at 800 K. The positive figure of merit (ZT) value of $RbAuBr_3$ and $RbAuBr_4$ demonstrate that the nature of both compounds is p-type.[62] The high ZT values indicate the potential of materials for thermoelectric devices.[63] It is noted that $RbAuBr_3$ exhibit high ZT values as compared to $RbAuBr_4$, which confirms it as a potential candidate for future thermoelectric devices.

Conclusions

Full potential linearized augmented plane wave method combined with modified Becke-Johson potential is used to study the physical properties of lead-free $RbAuBr_3$ and $RbAuBr_4$ perovskites. Optimized lattice parameters are used to compute the required properties. A semiconductor nature is observed for both materials, which is further confirmed by the density of states graphs. The optical and thermoelectric response is also evaluated. High absorption and low energy loss are observed for both materials. Transport properties show maximum electrical and minimum thermal conductivity for both perovskites. A very high ZT value of 0.96 is

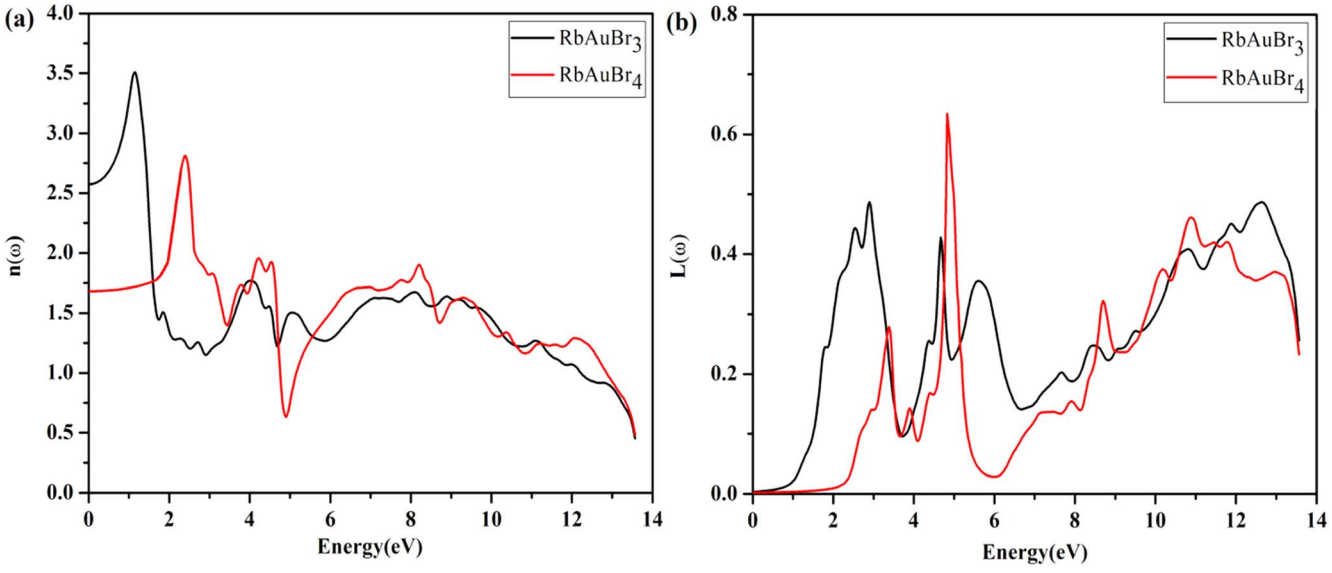

Figure 6. Calculated (a) refractive index and (b) energy loss of $RbAuBr_3$ and $RbAuBr_4$.

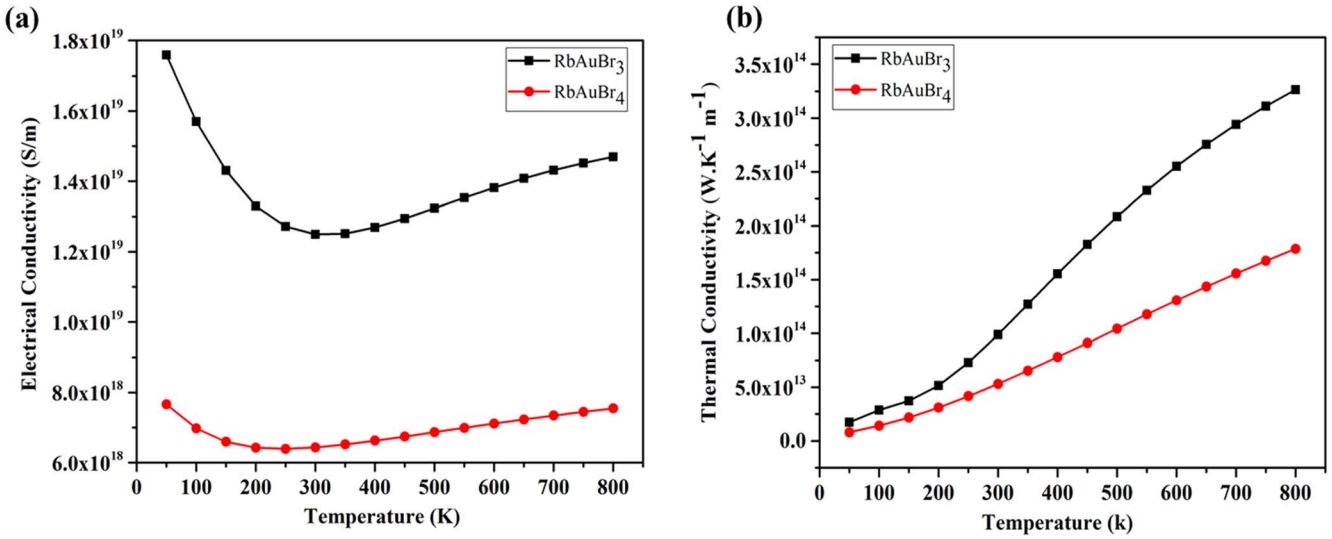

Figure 7. (a) Electrical conductivity and (b) thermal conductivity of $RbAuBr_3$ and $RbAuBr_4$.

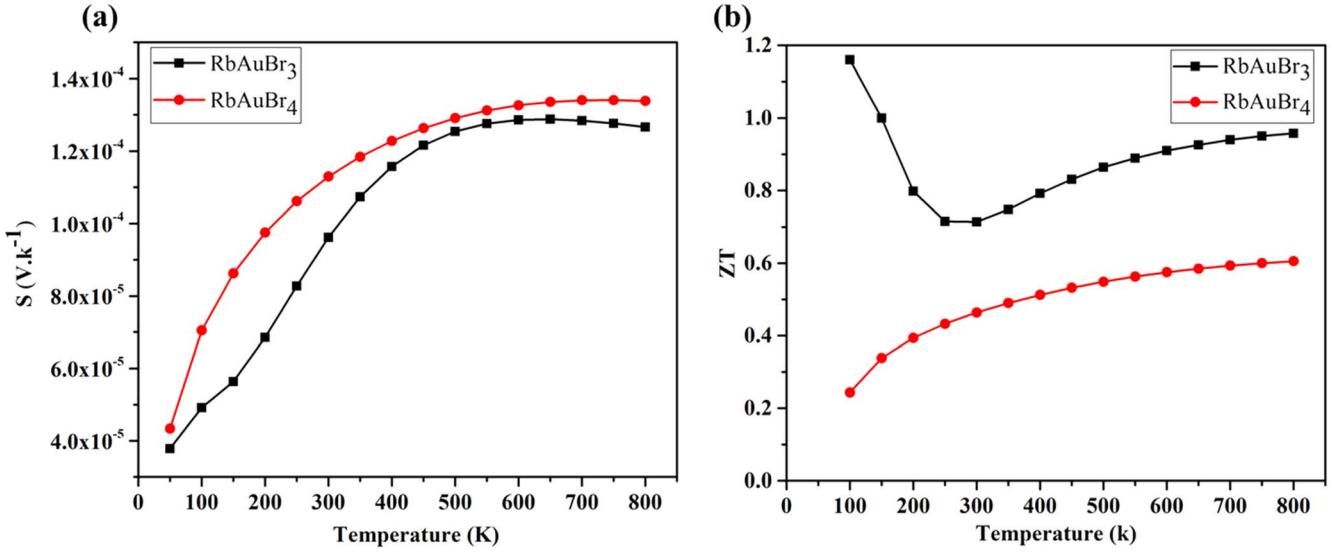

Figure 8. (a) Seebeck coefficient and (b) figure of merit for $RbAuBr_3$ and $RbAuBr_4$.

obtained for $RbAuBr_3$, which is the confirmation of using the studied perovskite in renewable energy applications.

Acknowledgments

The authors extend their appreciation to the Research Center for Advanced Materials Science (RCAMS), King Khalid University, Saudi Arabia, for funding this work under grant number RCAMS/KKU/013–22.

ORCID

Junaid Munir https://orcid.org/0000-0002-8347-2622
Quratul Ain https://orcid.org/0000-0002-1496-9547

References

1. C. Noguera, *Physics and chemistry at oxide surfaces* (Cambridge)(Cambridge University Press) (1996).
2. Q. Mahmood, U. E. Hani, T. I. Al-Muhimeed, A. A. AlObaid, B. U. Haq, G. Murtaza, T. H. Flemban, and H. Althib, *J. Phys. Chem. Solids*, **155**, 110117 (2021).
3. R. Sharma, A. Dey, S. A. Dar, and V. Srivastava, *Computational and Theoretical Chemistry*, **1204**, 113415 (2021).
4. Q. Ain, H. Ullah, and J. Munir, *Materials Science and Engineering: B*, **287**, 116136 (2023).
5. K. Fatima, Q. Ain, L. Mohammed, M. Jamil, A. M. Khan, M. Yousaf, and J. Munir, *Physica B*, **631**, 413688 (2022).
6. M. Nadeem, M. U. Din, H. T. Naeem, Q. Ain, and J. Munir, *ECS J. Solid State Sci. Technol.*, **11**, 033009 (2022).
7. J. Munir, A. S. Jbara, Q. Ain, K. Fatima, N. A. Noor, H. Naeem, M. Jamil, and M. Yousaf, *Physica B*, **618**, 413181 (2021).
8. M. E. Lines and A. M. Glass, *Principles and applications of ferroelectrics and related materials* (Oxford, UK)(Oxford University Press) (2001).
9. W. H. Kao, S. L. Haberichter, and K. R. Bullock, *J. Electrochem. Soc.*, **139**, L105 (1992).
10. O. Auciello, J. F. Scott, and R. Ramesh, *Phys. Today*, **51**, 22 (1998).
11. P. Schouwink, M. B. Ley, A. Tissot, H. Hagemann, T. R. Jensen, Ľ. Smrčok, and R. Černý, *Nat. Commun.*, **5**, 1 (2014).
12. M. A. Green, A. Ho-Baillie, and H. J. Snaith, *Nat. Photonics*, **8**, 506 (2014).
13. Z.-K. Tan, R. S. Moghaddam, M. L. Lai, P. Docampo, R. Higler, F. Deschler, M. Price, A. Sadhanala, L. M. Pazos, and D. Credgington, *Nat. Nanotechnol.*, **9**, 687 (2014).
14. H. Dong, C. Zhang, X. Liu, J. Yao, and Y. S. Zhao, *Chem. Soc. Rev.*, **49**, 951 (2020).
15. A. Kojima, K. Teshima, Y. Shirai, and T. Miyasaka, *J. Am. Chem. Soc.*, **131**, 6050 (2009).
16. F. Sahli et al., *Nat. Mater.*, **17**, 820 (2018).
17. M. V. Kovalenko, L. Protesescu, and M. I. Bodnarchuk, *Science*, **358**, 745 (2017).
18. J. Chen, S. Zhou, S. Jin, H. Li, and T. Zhai, *J. Mater. Chem. C*, **4**, 11 (2016).

19. M. Roknuzzaman, K. K. Ostrikov, H. Wang, A. Du, and T. Tesfamichael, *Sci. Rep.*, **7**, 1 (2017).
20. M. Roknuzzaman, K. K. Ostrikov, K. C. Wasalathilake, C. Yan, H. Wang, and T. Tesfamichael, *Org. Electron.*, **59**, 99 (2018).
21. V. T. Tiong, N. D. Pham, T. Wang, T. Zhu, X. Zhao, Y. Zhang, Q. Shen, J. Bell, L. Hu, and S. Dai, *Adv. Funct. Mater.*, **28**, 1705545 (2018).
22. P. Zhang, J. Yang, and S.-H. Wei, *J. Mater. Chem. A*, **6**, 1809 (2018).
23. N. K. Noel, S. D. Stranks, A. Abate, C. Wehrenfennig, S. Guarnera, A.-A. Haghighirad, A. Sadhanala, G. E. Eperon, S. K. Pathak, and M. B. Johnston, *Energy Environ. Sci.*, **7**, 3061 (2014).
24. P. Luo, W. Xia, S. Zhou, L. Sun, J. Cheng, C. Xu, and Y. Lu, *The journal of physical chemistry letters*, **7**, 3603 (2016).
25. C. Eames et al., *Nat. Commun.*, **6**, 1 (2015).
26. J. Liang, C. Wang, Y. Wang, Z. Xu, Z. Lu, Y. Ma, H. Zhu, Y. Hu, C. Xiao, and X. Yi, *J. Am. Chem. Soc.*, **138**, 15829 (2016).
27. C. F. J. Lau, X. Deng, Q. Ma, J. Zheng, J. S. Yun, M. A. Green, S. Huang, and A. W. Ho-Baillie, *ACS Energy Lett.*, **1**, 573 (2016).
28. J. S. Niezgoda, B. J. Foley, A. Z. Chen, and J. J. Choi, *ACS Energy Lett.*, **2**, 1043 (2017).
29. R. J. Sutton, G. E. Eperon, L. Miranda, E. S. Parrott, B. A. Kamino, J. B. Patel, M. T. Hörantner, M. B. Johnston, A. A. Haghighirad, and D. T. Moore, *Adv. Energy Mater.*, **6**, 1502458 (2016).
30. L. A. Frolova, D. V. Anokhin, A. A. Piryazev, S. Y. Luchkin, N. N. Dremova, K. J. Stevenson, and P. A. Troshin, *The journal of physical chemistry letters*, **8**, 67 (2017).
31. M. U. Din, J. Munir, M. Jamil, M. Saeed, and Q. Ain, *Physica B*, **627**, 413533 (2022).
32. A. S. Jbara, J. Munir, M. Yousaf, and M. Saeed, *J. Opt. Soc. Am. A*, **38**, 940 (2021).
33. A. S. Jbara, J. Munir, B. U. Haq, and M. Saeed, *Appl. Opt.*, **59**, 3751 (2020).
34. P. Liu, N. Han, W. Wang, R. Ran, W. Zhou, and Z. Shao, *Adv. Mater.*, **33**, 2002582 (2021).
35. M. U. Din, Q. Ain, M. Yousaf, and J. Munir, *Mater. Sci. Semicond. Process.*, **152**, 107081 (2022).
36. A. Mousa, M. Abu-Jafar, D. Dahliah, R. Shaltaf, and J. Khalifeh, *J. Electron. Mater.*, **47**, 641 (2018).
37. A. Radzwan, R. Ahmed, A. Shaari, Y. X. Ng, and A. Lawal, *Chin. J. Phys.*, **56**, 1331 (2018).
38. M. S. Khan, B. Gul, B. Ahmad, G. Khan, S. A. Khattak, T. Khan, M. Ajaz, S. Zulfiqar, and F. Wahab, *Mater. Sci. Semicond. Process.*, **144**, 106577 (2022).
39. D. Koller, F. Tran, and P. Blaha, *Physical Review B*, **85**, 155109 (2012).
40. G. K. Madsen and D. J. Singh, *Comput. Phys. Commun.*, **175**, 67 (2006).
41. X. Jiang, C. Ban, L. Li, C. Wang, W. Chen, and X. Liu, *AIP Adv.*, **11**, 055120 (2021).
42. V. Srivastava, N. Kaur, R. Khenata, and S. A. Dar, *J. Magn. Magn. Mater.*, **513**, 167107 (2020).
43. V. L. Solozhenko, E. G. Solozhenko, and C. Lathe, *Solid State Commun.*, **137**, 533 (2006).
44. A. Kundu, S. Ghosh, R. Banerjee, S. Ghosh, and B. Sanyal, *Sci. Rep.*, **7**, 1 (2017).
45. G. Rehman, M. Shafiq, R. Ahmad, S. Jalali-Asadabadi, M. Maqbool, I. Khan, H. Rahnamaye-Aliabad, and I. Ahmad, *J. Electron. Mater.*, **45**, 3314 (2016).
46. M. Fox, "Optical Properties of Solids." *American Journal of Physics*, **70**, 1269 (2002).
47. L. V. Keldysh, A. A. Maradudin, and D. Kirzhnitz, *The dielectric function of condensed systems* (Amsterdam)(Elsevier) (2012).
48. P. Grosse and V. Offermann, *Appl. Phys. A*, **52**, 138 (1991).
49. G. Orudjev and N. Ismayilova, *Adv. Phys. Res.*, **1**, 37 (2019).
50. J. Sun, X.-F. Zhou, Y.-X. Fan, J. Chen, H.-T. Wang, X. Guo, J. He, and Y. Tian, *Physical Review B*, **73**, 045108 (2006).
51. E. Holmström, A. Kuronen, and K. Nordlund, *Physical Review B*, **78**, 045202 (2008).
52. S. A. Khandy and D. C. Gupta, *RSC Adv.*, **6**, 48009 (2016).
53. S. Singh, *Phys. Scr.*, **65**, 167 (2002).
54. G. K. Madsen, J. Carrete, and M. J. Verstraete, *Comput. Phys. Commun.*, **231**, 140 (2018).
55. B. Szpunar, J. I. Ranasinghe, L. Malakkal, and J. A. Szpunar, *J. Phys. Chem. Solids*, **146**, 109636 (2020).
56. M. Jonson and G. Mahan, *Physical Review B*, **21**, 4223 (1980).
57. G. J. Snyder and A. H. Snyder, *Energy Environ. Sci.*, **10**, 2280 (2017).
58. C. Y. Ho, R. W. Powell, and P. E. Liley, *J. Phys. Chem. Ref. Data*, **1**, 279 (1972).
59. S. A. Khandy, I. Islam, D. C. Gupta, R. Khenata, A. Laref, and S. Rubab, *Mater. Res. Express*, **5**, 105702 (2018).
60. J. de Boor and E. Müller, *Rev. Sci. Instrum.*, **84**, 065102 (2013).
61. G. Mahan, *J. Appl. Phys.*, **65**, 1578 (1989).
62. B. J. Baliga, *IEEE Electron Device Lett.*, **10**, 455 (1989).
63. V. Fiorentini, R. Farris, E. Argiolas, and M. B. Maccioni, *Phys. Rev. Mater.*, **3**, 022401 (2019).